# NUMERICAL CALCULATIONS OF ACOUSTIC EMISSION

John A. Johnson

Idaho National Engineering Laboratory
EG&G Idaho, Inc.
Idaho Falls, Idaho 83415

## INTRODUCTION

A computer program [1] which solves the partial differential equations for sound propagation numerically is applied to the study of problems in acoustic emission. The program uses finite difference techniques to calculate sound fields due to distributions of sources in complex geometries in two dimensions. The potential to handle more complex geometries and to model more realistic sources is the main advantage of this type of calculation over the analytic calculations. The main disadvantage of the numerical technique is the cost of obtaining results since a large main frame computer or supercomputer is required.

In this paper the fields due to a simple source in a planar geometry are calculated and compared to the analytic results using the methods developed by Pao and his collaborators [2,3]. The purpose of these calculations is to test the feasibility of the code for calculations of acoustic emissions and to determine the limitations by comparing it with the Green's function or generalized ray theory results. Further calculations in more complex geometries which cannot be handled by the Green's function method are planned, including the effect of sources near or at the tip of a crack and the effect of geometric distortions due to plastic strain in a sample in a tension test.

## METHOD OF CALCULATION

In the finite difference method, the partial differential equations describing the system are approximated by finite differences in both space and time. The physical system to be analyzed is divided up into small quadrilateral zones. The four zones surrounding the grid point labeled (I,J) are shown in Fig. 1 with their respective stresses. The size of the zones should ideally be less than about 1/10 of the shortest wavelength of interest. Economic considerations may require some compromise of this ideal.

The stress in each zone is calculated from the integrated strain rate in that zone, which is determined by the velocities of the points at the four corners of the zone. Then the acceleration of the points of the mesh

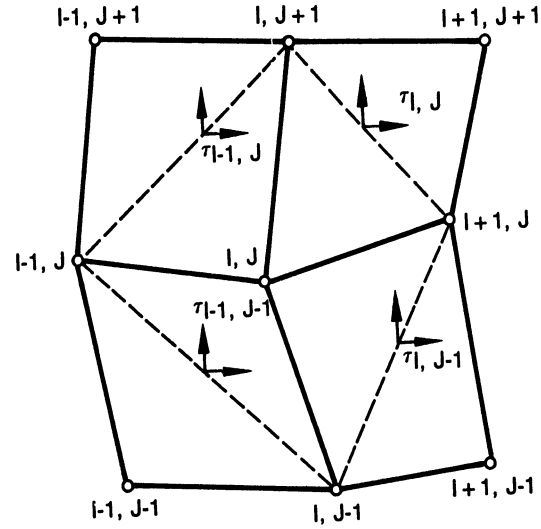


Fig. 1. around a mesh point in a finite difference grid.

are calculated from the stresses around that point and integrated in time using a time-centered formulation to find new velocities and displacements from the previous values. Boundaries are represented by special values of the stresses or velocities corresponding to the desired physical situation. For example, a free boundary is modeled by having zero stress on the sides of a zone on the boundary. In this paper the acoustic emission on the surface is modeled by putting a time dependent stress on the sides of the relevant zones.

## COMPARISON TO GREEN'S FUNCTION METHOD

The Green's function method, also known as the theory of generalized rays, was first applied by geophysicists for the study of stress waves generated by earthquakes. Rays from the source are traced to the locations of the receiver. The transient response of each ray is calculated from the inverse Laplace transform of a combination of integrals which depend on the source, receiver, and ray path, including mode conversions at the boundaries of the plate [2,3]. The solution is then the sum of the transients for each individual ray which arrives during the time of interest.

The Green's function analysis uses an exact heaviside time function for a point force. However, such a forcing function in a finite difference scheme would contain high-frequency components in both space and time which would produce waves of very short wavelengths. Such short wavelengths would be too small for any mesh and would result in numerical noise. Thus the forcing function must be approximated by a function that is bandwidth limited and of finite size. The bandwidth is chosen so that the equivalent minimum wavelength is ten times larger than the zone size:

$$F = F_o \left(1 - e^{-t^2/T^2}\right)$$

This function has a 20 dB bandwidth of:

$$f = \frac{\sqrt{\ln 10}}{\pi T} = 0.48/T$$

Similarly the spatial width of the forcing function in the analytic calculations is zero, i.e., the spatial part is a delta function and acts at a point. Again the numerical scheme does not allow such a distribution and requires the source to be spread over several zones.

These limitations of the numerical finite difference method are not really all that deleterious since in real experimental situations the sources, and certainly the receivers, do have limited bandwidth. Some sources, however, are point-like in space on the scale of the discretization used here. A cracking inclusion in a metal, for example, could have dimensions much smaller than 0.2 mm, the zone size in this calculation.

Modeling the forcing function for the finite difference method results in some differences between the results of the numerical method and the Green's function method. The rise and fall times of the calculated displacements in the Green's function calculations can be zero, corresponding to the input step function force. In the numerical calculation the rise and fall times are limited by the bandwidth of the input force. A second effect is to lower the displacement amplitude in the numerical calculation, especially when the Green's function result is a step displacement. The finite source size has a similar effect of smearing out the wave form since the time of arrival of a pulse is different, depending on what part of the source it came from. This also tends to reduce the peak displacement amplitudes when compared to the Green's function solutions.

The Green's function solutions can be extended to finite size and limited bandwidth sources using standard filtering and integration techniques.

Sample Acoustic Emission Problem

In order to test the method, a point normal heaviside force on the surface of a plate is modeled using finite difference methods. A schematic of the problem is shown in Fig. 2. The exact solution to this problem can be calculated using Green's functions and has been verified experimentally [2-4]. Thus the results from the finite difference calculations can be compared and verified with confidence.

Ceranoglu [5] has presented in graphical form the results of just such a problem. The geometry and material properties in this study have been chosen to match those used in his calculation. Ceranoglu's data are in normalized nondimensional form in both time and displacement. To simplify the comparison, the longitudinal wave speed and the plate thickness have been chosen to have equal magnitudes (6 mm/μs and 6 mm) so that the normalized time and the real time in microseconds are the same. The shear wave speed was then chosen to be equivalent to that used by Ceranoglu, who used a longitudinal-to-shear wave sound speed ratio of $\sqrt{3}$ (3.46 mm/μs).

The numerical calculation actually requires the bulk and the shear moduli and the density. For a density approximately that of steel (8.0 g/cm$^3$), the required bulk and shear moduli to obtain sound speeds above are 1.60 and 0.96 Mbars respectively.

The normalized nondimensional displacement response used by Ceranoglu is determined by multiplying the actual displacement response by

$$\text{Nomalized Displacement} = \frac{\pi\mu h^2}{F_o} \times \text{displacement}$$

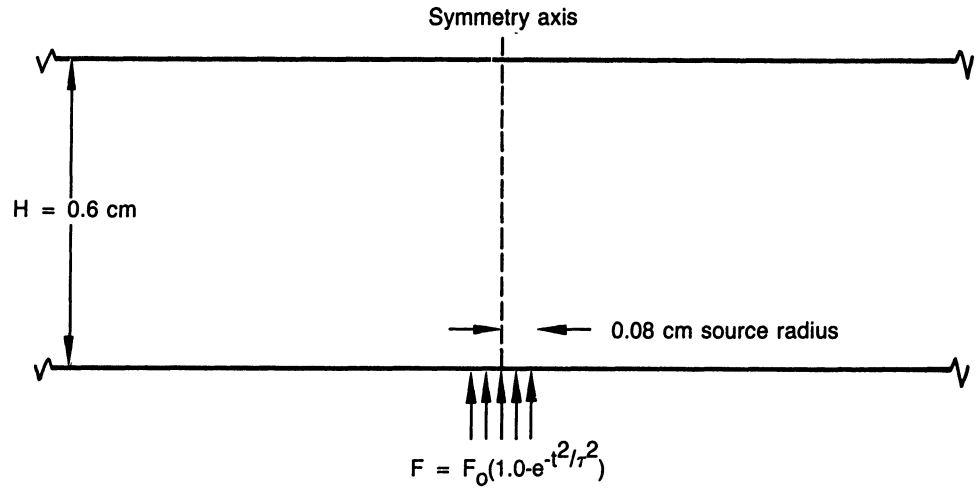


Fig. 2. Acoustic emission in a plate due to a source on the surface.

where h is the plate thickness, $\mu$ is the shear modulus, and $F_0$ is the strength of the force. In the finite difference calculation the point source is modeled by a uniform normal stress of radius 0.8 mm and strength $10^{-4}$ Mbars. The force is the area of this circle times the stress, or $2.0 \times 10^6$ dynes. Then the final conversion factor for determining the normalized displacement is:

Normalized displacement = $0.54 \times 10^6$ x displacement in cm

The mesh consisted of zones of 0.2 mm on a side. The height of the mesh was chosen to be 6 mm, as noted above. The radial size of the mesh was chosen so that reflections from the far boundary would not return to points in a radius of 12 mm during the time of interest (5 $\mu$s). The zone size of 0.2 mm then requires that the minimum wavelength in the problem be greater than about 2.0 mm or 10 times the zone size. In Table 1 the 20 dB bandwidth and the shear wavelength in mm and in zone lengths are given for various values of the risetime used in the calculation. From this table, the forcing function with a risetime of 0.32 $\mu$s should be adequate for the a mesh with zones 0.2 mm on a side.

Comparison of the Finite Difference and Green's Function Calculations

The finite difference program results are shown in graphical form in Figs. 3 through 6. The left side of the plots is the axis of symmetry,

Table 1. Forcing Function Bandwidth and Shear Wavelength for several values of Forcing Function Rise Time.

| Rise Time Micros | Bandwidth MHz | Wavelength mm | Wavelength Zone Lengths |
|---|---|---|---|
| 0.45 | 1.1 | 3.2 | 16.0 |
| 0.32 | 1.5 | 2.3 | 11.5 |
| 0.14 | 3.4 | 1.0 | 5.0 |

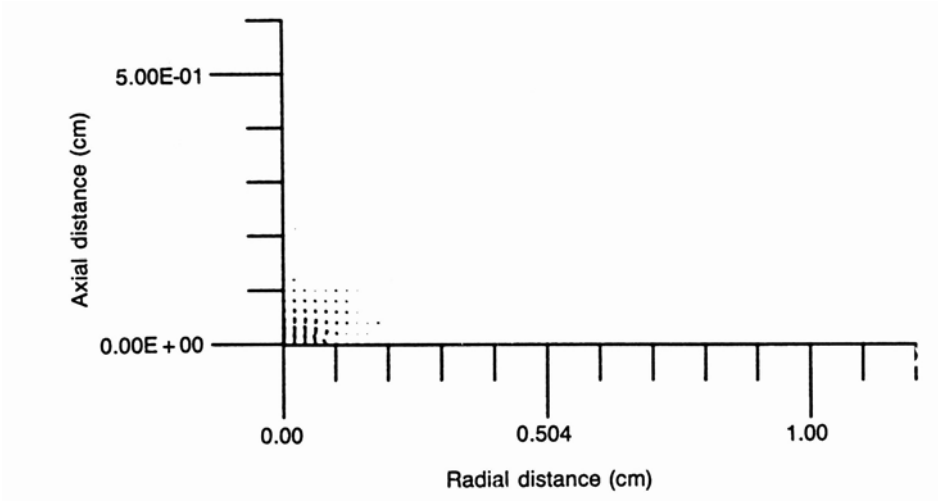


Fig. 3. Vector field plot at 0.2 μs. The left axis is the axis of symmetry. The horizontal axis is the radial distance.

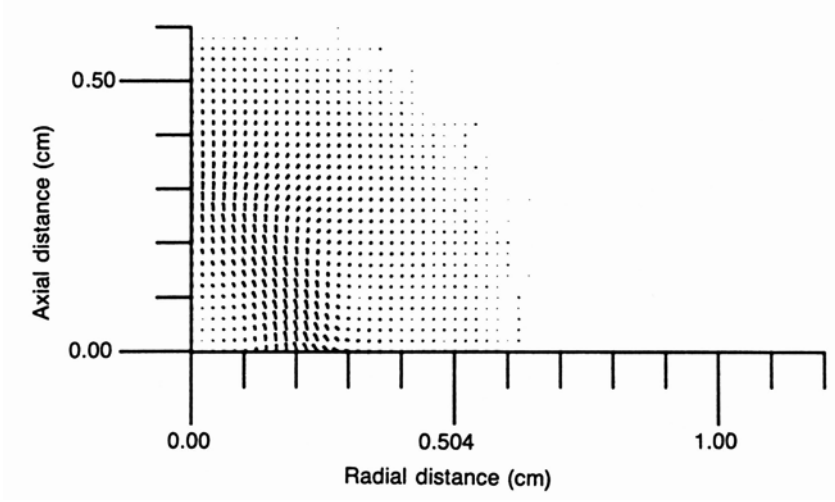


Fig. 4. Velocity field plot at 1.0 μs.

corresponding to the center of Fig. 2. Each plot is a snapshot of the velocity vector field at various times. In Fig. 3 the field at 0.2 μs is confined to the lower left corner of the grid, next to the source. In succeeding figures waves propagate out from the source on the axis. The longitudinal wave has reached the top of the plate while the shear wave forms an arc at 1.0 μs in Fig. 4. Along the radial (horizontal) axis the arc is distorted by the Rayleigh surface wave which has a slightly slower sound speed than the shear wave. The shear wave has reached the top of the plate in Fig. 5 and can be seen reflecting off the top in Fig. 6 forming a second arc.

For comparison with the Green's function calculations, plots of the displacement as a function of time can be made at any point in the grid. Ceranoglu [5] has shown a plot of the displacement versus time for several

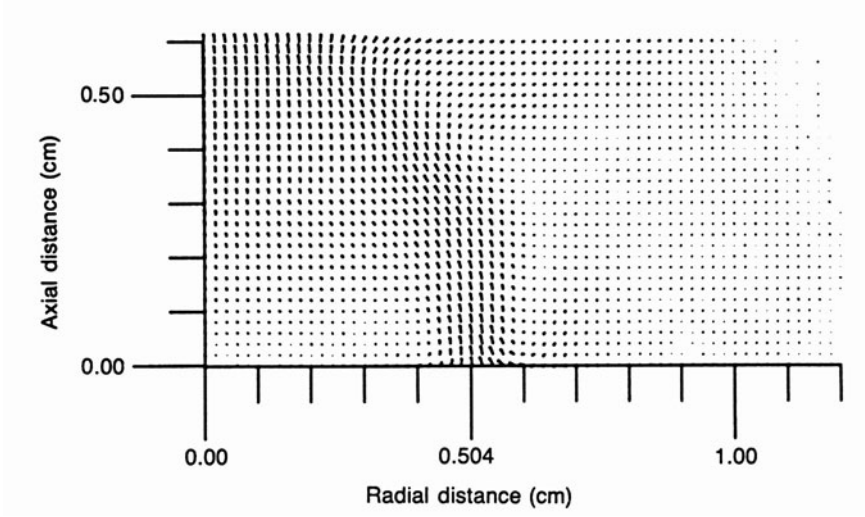


Fig. 5. Velocity field plot at 2.0 μs.

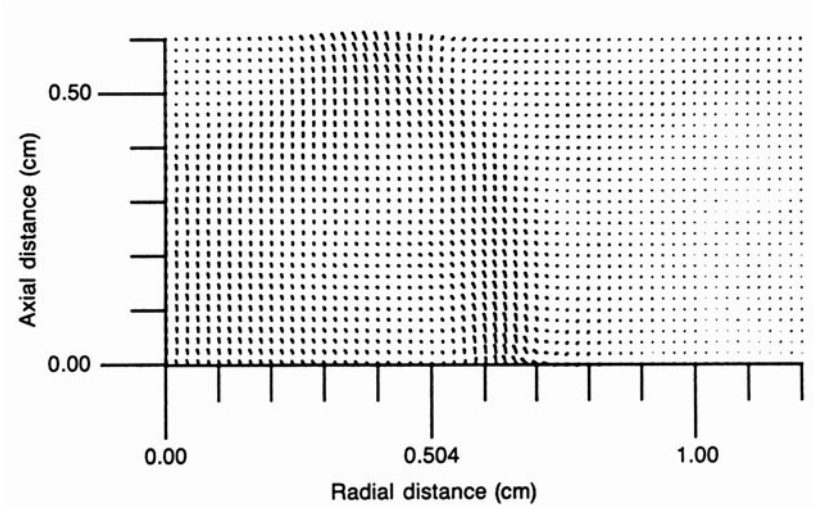


Fig. 6. Velocity field plot at 2.4 μs.

points in the plate. In Fig. 7 one of his plots is reproduced, giving the displacement on the bottom of the plate (same side as the source) at a radial distance of twice the thickness of the plate. This corresponds to a radius of 12 mm in the finite difference calculations.

In Figs. 8 and 9 the radial displacements versus time for two different source rise times (0.32 and 0.14 μs) are shown. Similar plots for the axial displacements are displayed in Figs. 10 and 11. These plots are smoothed versions of the displacements given in Fig. 7, actually corresponding to the convolution of the displacements from the Green's function calculations and the source time function, integrated over the source function. In all the plots the small longitudinal wave arrives at 2.0 μs. The normalized amplitude for the radial component is approximately 0.036, corresponding to $0.67 \times 10^{-7}$ Mbars, more than twice that shown in Figs. 8 and 9. The dip at about 3.8 μs, marked with an R

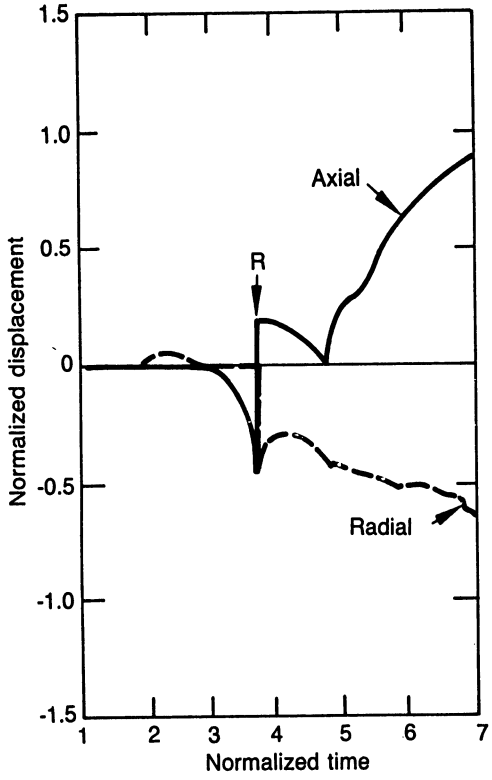


Fig. 7. Green's function calculation of the displacement versus time for a point on the same side of the plate at the source, at a radial distance of twice the thickness of the source.

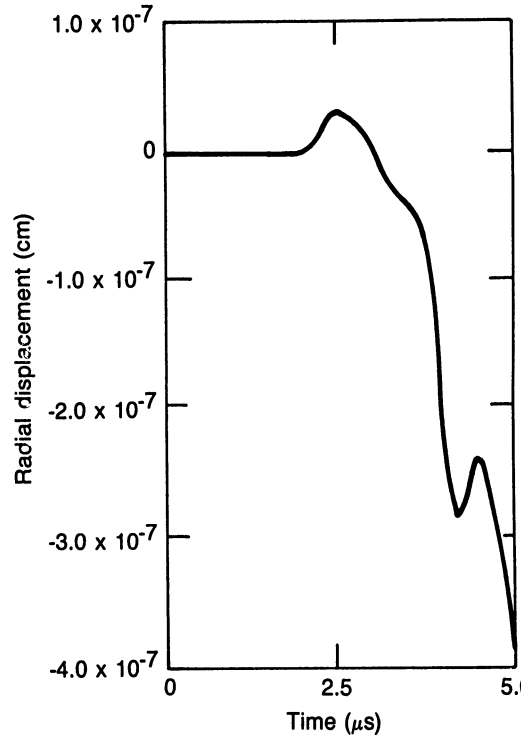


Fig. 8. Radial displacement calculated using finite difference methods for a source risetime of 0.32 μs.

in Fig. 7, corresponds to the arrival of the Rayleigh wave. This, and the rise after 4.0 μs, is reproduced in a smoothed fashion in Figs. 8 and 9.

The axial component of the displacement in the finite difference calculations also follows the Green's function results. A very small longitudinal component arrives at 2.0 μs, followed by the Rayleigh wave component. The positive excursion in Fig. 7 just after the Rayleigh wave arrival has an amplitude of about 0.15 normalized units, corresponding to $2.8 \times 10^{-7}$ Mbar. From the finite difference method values of $1.4 \times 10^{-7}$ and $1.6 \times 10^{-7}$ are obtained in Figs. 10 and 11.

In summary, the effect of the finite rise time and finite source size in the numerical calculations is a smoothed version of the Green's function results with significantly lower amplitude. The plots with the faster rise times more closely reproduce the sharp features of the Green's function results as expected.

## CONCLUSION

Finite difference calculations of acoustic emission on the surface of a plate have been shown to be equivalent to the Green's function or generalized ray theory results within certain limitations resulting from a reduced frequency bandwidth and finite source size in the numerical calculations. The next steps include simulating a buried source of

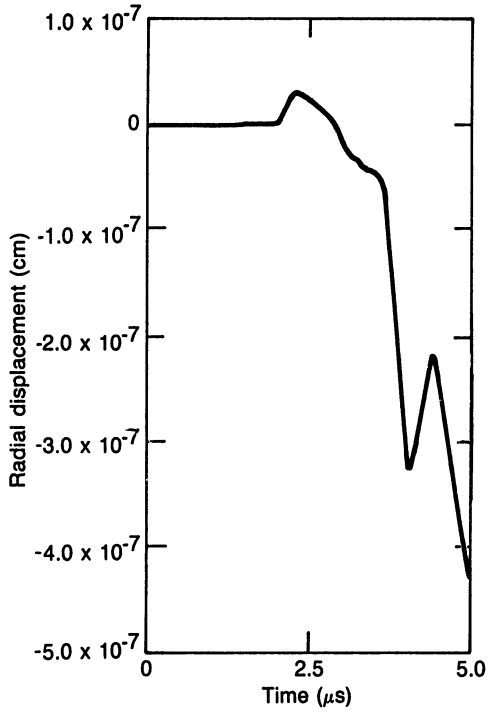


Fig. 9. Radial displacement for a source risetime of 0.14 μs.

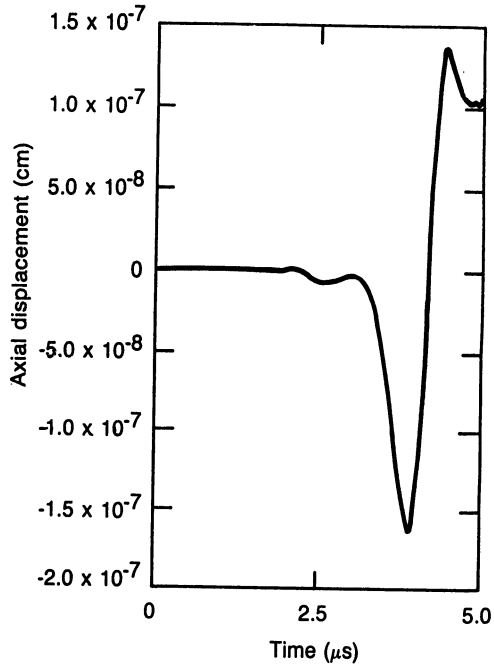


Fig. 10. Axial displacement for a source risetime of 0.32 μs.

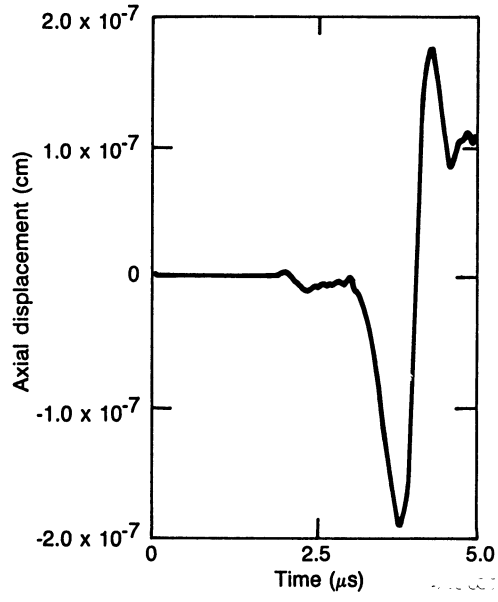


Fig. 11. Axial displacement for a source risetime of 0.14 μs.

acoustic emission and comparing the results to the analytic theory and to a model of more complex geometries that the analytic theory is not capable of handling. These include sources near or at a crack tip with the complex boundary conditions of the crack and accounting for large strains in the plate, similar to what might be encountered in tension tests of ductile specimens.

## ACKNOWLEDGMENTS

This work is supported by the U. S. Department of Energy, Office of Energy Research, Office of Basic Energy Sciences under DOE Contract No. DE-AC07-76ID01570.

## REFERENCES

1. J. A. Johnson, "Numerical Calculations of Ultrasonic Fields: Transducer Near Fields", J. of NDE 3, 27 (1982).
2. Pao, Gajewski, and Ceranoglu, "Acoustic Emission and Transient Waves in an Elastic Plate", JASA 65, 96 (1979).
3. A. N. Ceranoglu, "Acoustic Emission and Propagation of Elastic Pulses in a Plate", Ph.D. Thesis, Cornell University (1979).
4. J. E. Michaels, T. E. Michaels, and W. Sachse, "Applications of Deconvolution to Acoustic Emission Signal Analysis", Materials Evaluation 39, 1032-1036 (1981).
5. A. N. Ceranoglu, op. cit., 137.